Progress In Electromagnetics Research C, Vol. 97, 123–137, 2019

Estimation of Three-Phase Currents in Overhead Power Line Conductors Using Numerical Model of Magnetic Fields

Prasad Shrawane* and Tarlochan S. Sidhu

Abstract—This paper proposes a new method of calculating currents in three-phase overhead medium and high voltage networks by measuring the magnetic fields generated in the close vicinity of the power line conductors. A mathematical model for magnetic fields is presented in the form of second order partial differential equations that are derived from Maxwell's equation. The analysis of the magnetic field surrounding overhead conductors is performed using Finite Element Method. The least squares method is used for the formulation of equations for estimating currents from the measured magnetic fields for each phase. A computational program for detail analysis is developed in MATLAB. A plan for measurement points is developed for triangular arrangement of conductors. Field measurement with increased number of measuring points gives better results than those with the single points.

1. INTRODUCTION

Measurement of instantaneous values of current and voltage is very important for power systems protection, control, and stability considering the increasing trend of bidirectional power flow in distribution and sub-transmission networks. It is performed by traditional current transformers (CT) or electronic CTs and voltage transformers. Traditional CTs are ferrite core window-type with wound conductor. Their major drawback is saturation and heating which occurs because of the peak magnetizing currents generated during transients, or faults. To avoid this problem, a higher ratio CT can be used which results into higher price. Moreover, these CTs need electrical isolation and grounding of the system for installation, maintenance and repair [1, 2]. They are deployed at generation, transmission, and distribution substation in most cases. Recently there is an increasing trend of using the electronic CTs for current measurement considering low operational cost and ease of integration to automation. They consist of sensors which sense the magnetic field and transduce it into the corresponding values of currents. A noninvasive design of the current transformers reduces all risks and electrical hazards in electrical isolation procedure and decrease the frequency and time of outage. Therefore, this research aims at calculating the instantaneous values of currents from measured magnetic field for a three-phase overhead power system. As an initial step to achieve this aim, it was necessary to first study, simulate, and analyse the magnetic field produced around current carrying conductors. Various research articles were reviewed to find a suitable method for numerical approximation of magnetic field.

It is difficult to find the exact solution to the magnetic field from the equations. There are a few numerical methods used by researchers to reach the near accurate approximation of the actual magnetic field. These methods include [3–5] Finite Difference Time Domain method (FDTD), Method of Moments (MoM), Variational Iteration Method (VIM), and Finite Element Method (FEM). In the past, many research teams have shown interest in exploring various methods to calculate the magnetic field generated by power line conductors and use it for various applications. They used numerical

Received 16 August 2019, Accepted 18 November 2019, Scheduled 4 December 2019
* Corresponding author: Prasad Shrawane (prasad.shrawane@uoit.ca).
The authors are with the Department of Electrical and Computer Engineering, The University of Ontario Institute of Technology, Canada.

and semi-numerical techniques to approximate magnetic fields and validated their methods with the actual measured values. Hameyer et al. [6] applied a combination of semi-numerical method and FEM to calculate the magnetic field in 150 kV overhead transmission lines in Belgium. The mathematical model was developed for Aluminium Core Steel Reinforced (ACSR) conductors in both two- and three-dimensions using a cartesian coordinates system. The values calculated by using the FEM model were compared with the actual measured values with the help of Holaday Industries model HI-3604. The meter used for field measurement consists of a circular coil and a fibre-optic receiver with a non-conductive tripod stand. The team found that the results of the FEM model were in agreement with measured values by the meter for a two-dimensional model. In another research [7], Farah et al. performed a comparative study to find the accurate estimation of magnetic field at the surface of overhead transmission line conductors. This team applied three methods for the computation of magnetic field, namely, method of successive images, FEM using a spatial transformation, also known as Kelvin Transformation, and the traditional FEM method. The focus of their study was a 525 kV transmission line with ACSR conductors in Brazil. Their work proposed imposing virtual circular boundaries close to conductors and assuming the ground to be entirely in external transformed domain. This reduced the study domain of the FEM model and increased the computational accuracy. Pao-La-Or et al. [4, 8] presented a two-dimensional time varying finite element model for electromagnetic field approximation in the induction motor. It is found that the mathematical model is identical to that of transmission lines except that this work used the Newton-Raphson method combined with bi-conjugate gradient (BCG) method to reduce the computational time and achieve better convergence. They applied the Galerkin weighted residual method to derive the covariance matrix for the second order partial differential equation of magnetic field in two-dimensional plane. The numerical simulation for Maxwell's equations which was performed almost by every research team mentioned used FEM. But this was also explored using the FDTD method using Yee algorithm by Mismar [9] in which the author showed the application of this method for a square region with dimension of 5 cm. This method had limitations of accuracy and computational time because of restricted mesh size and smaller size of the matrix. Thus, successful efforts towards magnetic field modeling by various researchers motivated this research to use the FEM based modeling of magnetic fields in overhead distribution and transmission system.

It is observed that researchers have explored various sensing techniques to measure the magnetic field to give proportional values of currents to the maximum accuracy. These sensing techniques are based on principles such as Faraday's law of induction, Ohm's law of resistance, Faraday's effect and magnetic field sensing. Magnetic field sensors work on the principle of Faraday's law of induction [9–11]. They can sense both static and time varying magnetic fields. There are three basic configurations with magnetic sensors, open loop, closed loop, and a combination of the magnetic sensor with other sensors such as Hall Effect and Rogowski coil. The basic operating principle of Rogowski coil involves a mutual inductance between the primary single turn and secondary multiple turns. The output voltage is proportional to the derivative of current. Thus, it is an advantage over traditional current transformers, because it does not contain any ferromagnetic material [9, 10]. Hall Effect sensors [11, 12] are widely used in various applications for measuring currents from a few milliamperes to 100 A. Hall Effect was discovered by Edwin Hall in 1879. When a current carrying conductor is placed into a magnetic field, a proportional voltage is developed perpendicular to both the current and the magnetic field. This is the basic principle of Hall Effect. The Hall voltage is proportional to the vector cross product of current and the magnetic field. Fluxgate Sensor [13, 14] consists of ferromagnetic material wound with two coils, a drive, and a sense coil. It is based on the principle of magnetic induction. The name of the device comes from this "gating" of the flux that occurs when the core is saturated. When the measured field is present, a voltage is induced into the sensing coil at the second harmonics of the excitation frequency. This voltage proportional to the measured field is usually the sensor output, but some flux gates also work in the short-circuited mode to have current as the output. Magnetoresistive (MR) [15–17] sensors are used for current sensing or position, speed and angle sensing, as well as Earth's magnetic field sensing in compass applications. A Wheatstone bridge type construction of GMR sensor allows for the maximum and minimum resistances and accordingly measures the positive magnetic field. In addition, it allows for cancellation of temperature effects (thermal drifts) and also for a level of immunity to stray magnetic fields. The output of the Wheatstone bridge is fed to a differential amplifier and then through

the normal sensitivity and offset correction circuit and then to filter circuits. Moreover, this sensor overcomes the drawbacks of current sensing using other sensors mentioned previously.

This paper gives an FEM analysis for three-phase overhead power system networks for medium and high voltage levels. In further stage of the research, these results obtained for the magnetic field are used to calculate the currents for three-phases by applying a least square regression method. Section 2 gives detailed steps of developing the mathematical model of magnetic field in the case of triangular arrangement of three-phase conductors. Section 3 gives finite element formulation of the model to achieve more accurate approximation with ease of computation. Various details such as, discretization, boundary conditions, simulation parameters for programming are explained in Subsections 3.1 and 3.2. Section 4 describes the systematic approach towards capturing the magnetic field at specific distances from three-phase conductors. A method of linear regression analysis is explained in Section 5, and it is implemented using MATLAB to estimate current values for each phase. Section 6 and Section 7 include simulation results for various combinations of measuring points for medium voltage (MV) and high voltage (HV) systems. Section 8 gives conclusions and discussion based on the results of simulation and modeling using FEM for current estimation.

2. MATHEMATICAL MODEL OF MAGNETIC FIELD

The magnetic field (B) generated surrounding a power line conductor carrying high current can be mathematically modeled with the help of the magnetic field intensity, H, by following Biot-Savart Law. Its adoption for a low frequency of 60 Hz is given as

$$B = \mu_0 H = \frac{\mu_0 I}{2\pi d} \text{ Wb/m}^2 \tag{1}$$

where μ_0 is the permeability of free space (air in this case). The above equation shows that the magnetic flux density is directly proportional to current. Therefore, measuring the flux density can get the value of current considering a uniform permeability of the medium.

The study of magnetic fields generated by multiple sources can be explored in detail by considering a set of three-phase medium voltage system with balanced three-phase voltages. The overhead structure can be of two types as shown in Fig. 1. Each of the three phases generates a magnetic field surrounding them because of the time-varying low frequency sinusoidal voltage source. In such a case, the resultant magnetic field at one single point in the surrounding is a function of distances from each phase conductor, time, magnitude of the time-varying current, and the phase angle. When all three phases have alternating currents $I_A(t)$, $I_B(t)$, and $I_C(t)$, then the magnetic field B_T at point P1 is a function

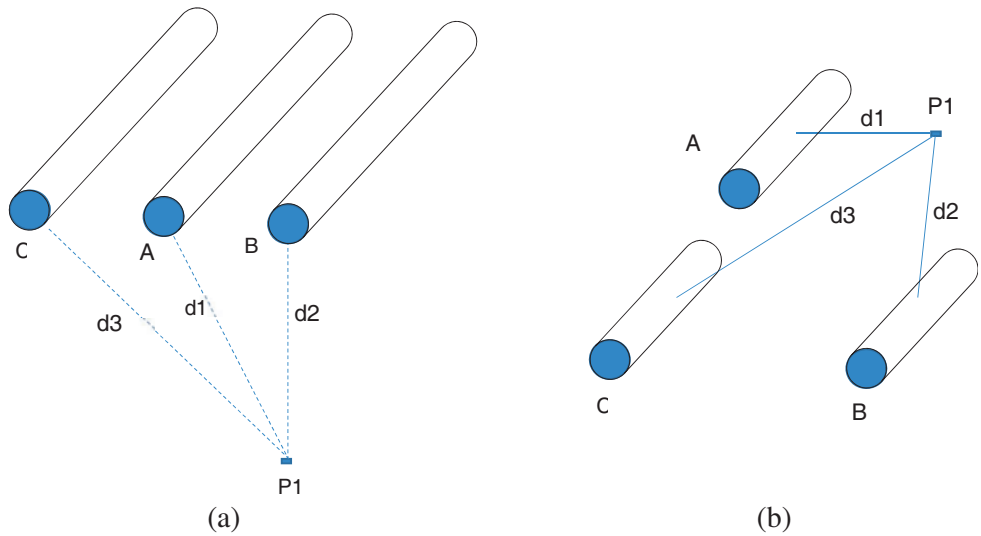

Figure 1. Three-phase overhead conductor arrangement.

of combined fields due to all three phases and can be written as

$$B_T = f\left\{B_A\left(I_A, \theta_A, t\right), B_B\left(I_B, \theta_B, t\right), B_C\left(I_C, \theta_C, t\right)\right\} \tag{2}$$

It is assumed that three phases are balanced with a phase difference of 120° at a frequency of 60 Hz. The resultant magnetic field at point P1 will be a vector addition of individual fields produced by three-phase currents varying with time and phase angle, θ, and is expressed as

$$B_{\mathrm{P1}}\left(I, t\right) = \sum_{t=1}^{t=n}\sum_{j=1}^{j=q}\left\{B_A\left(I_{Aj_\theta}, t\right) + B_B\left(I_{Bj_{\theta-120}}, t\right) + B_C\left(I_{Cj_{\theta+120}}, t\right)\right\} \tag{3}$$

The magnetic field density given in above equation is also represented as medium dependent Maxwell's first order differential equations. It is difficult to solve for time varying fields especially when solving boundary-value problems, as in the case of power line conductors. This difficulty is solved by decoupling the first order equations to obtain a wave equation which is a second-order differential equation. This equation is also known as Helmoltz's equation [6, 7]. Using this equation and following the Ampere's circuital Law, the second-order differential equation for magnetic field intensity is given as

$$\nabla^2 H - \sigma\mu\frac{\partial H}{\partial t} - \varepsilon\mu\frac{\partial^2 H}{\partial t^2} = 0 \tag{4}$$

where ε is the constant dielectric permittivity, μ the magnetic permeability, and σ the conductivity. For a time-varying field, the magnetic field intensity, H, is represented as

$$H = He^{j\omega t} \tag{5}$$

which modifies the first and second derivatives into

$$\frac{\partial H}{\partial t} = j\omega H \quad \text{and} \quad \frac{\partial^2 H}{\partial t^2} = -\omega^2 H \tag{6}$$

where ω is the angular frequency. Using Equation (6), Equation (1) can be rewritten into the following equation

$$\nabla^2 H - j\omega\sigma\mu H + \omega^2\varepsilon\mu H = 0 \tag{7}$$

This paper explores the magnetic field problem in a two-dimensional space. Therefore, applying the above equation to a two-dimensional XY plane to get

$$\frac{\partial}{\partial x}\left(\frac{1}{\mu}\frac{\partial H}{\partial x}\right) + \frac{\partial}{\partial y}\left(\frac{1}{\mu}\frac{\partial H}{\partial y}\right) - \left(j\omega\sigma - \omega^2\varepsilon\right)H = 0 \tag{8}$$

It is difficult to find the exact solution of Equation (8) analytically. Therefore, it can be solved using numerical methods on the space grids. Among the various methods of solving the space grid problems as mentioned previously, FEM is more powerful and versatile numerical technique for solving the complex problems which involve complex geometries and inhomogeneous media. Therefore, the problem of modeling the magnetic field for a three-phase overhead power line conductor is formulated using FEM and explained in the following section.

3. FINITE ELEMENT FORMULATION

To apply the finite element method, it is necessary to define dimensions of the region of magnetic field surrounding three-phase conductors. This research focuses on the medium voltage (MV) and high voltage (HV) overhead power system. Therefore, the specific height of conductors from ground, the radius of the circular region, and the distance between phase conductors are decided by following the standards of Utility Standards Forum (USF) that are followed by local distribution companies in Ontario, Canada. Accordingly, the overhead conductors considered for this research are Aluminium Core Steel reinforced (ACSR) single conductors [18, 19]. The diameter of each conductor for medium voltage is 355 mcm and 556 mcm for high voltage application. The clearances among three conductors are chosen from Tables 2–4 of the USF Standard [17]. A triangular structure is considered as shown in Fig. 2 with a horizontal spacing of 113 cm and the vertical spacing of 98 cm. A circular region of radius 200 cm surrounding three conductors placed at three corners of a triangle is considered for the finite element analysis.

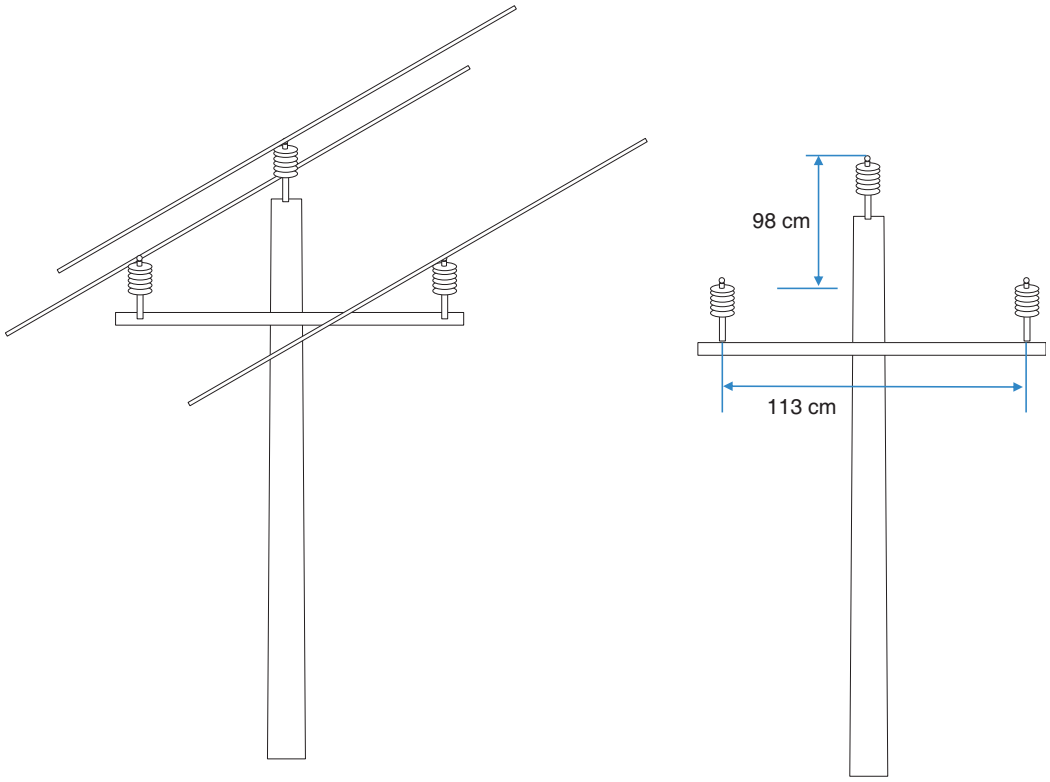

Figure 2. Triangular and horizontal arrangement of three-phase conductors.

3.1. Discretization

In a two-dimensional solution space, the circular region surrounding the power line conductor is discretized into finite elements of triangular shape with three nodes with each node having x and y coordinate as shown in Fig. 3. Therefore, each node will have a finite value of magnetic field intensity. Thus, the circular region is divided into many tiny nodes to form meshes. Each element at each node will have a finite magnetic field intensity which sums to the total intensity. Suppose that each node has an intensity of $H_e(x, y)$, then the total magnetic field intensity for the whole region is expressed as

$$H_T(x, y) \cong \sum_{e=1}^{N} H_e(x, y) \tag{9}$$

Assuming linear variation of the magnetic vector potential within each triangular finite element, the approximation of H_e can be represented by a polynomial [3] as

$$H_e(x, y) = a + bx + cy \tag{10}$$

Consider a triangular finite element shown in Fig. 3 with magnetic field intensity of H_{e1}, H_{e2} and H_{e3} and coordinates of three nodes as $n_1(x_1, y_1)$, $n_2(x_2, y_2)$, and $n_3(x_3, y_3)$. Then following the above Equation (10), the vector magnetic potential is obtained as:

$$\begin{bmatrix} H_{e1} \\ H_{e2} \\ H_{e3} \end{bmatrix} = \begin{bmatrix} 1 & x_1 & y_1 \\ 1 & x_2 & y_2 \\ 1 & x_3 & y_3 \end{bmatrix} \begin{bmatrix} a \\ b \\ c \end{bmatrix} \tag{11}$$

The coefficients, a, b, and c, are determined from above equation as:

$$\begin{bmatrix} a \\ b \\ c \end{bmatrix} = \begin{bmatrix} 1 & x_1 & y_1 \\ 1 & x_2 & y_2 \\ 1 & x_3 & y_3 \end{bmatrix}^{-1} \begin{bmatrix} H_{e1} \\ H_{e2} \\ H_{e3} \end{bmatrix} \tag{12}$$

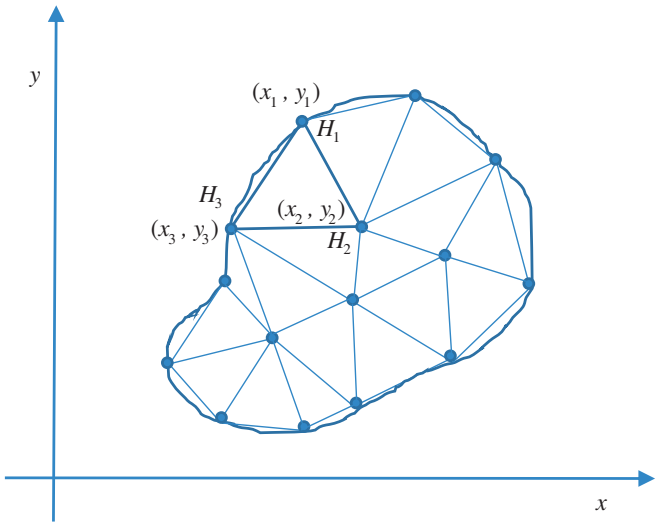

Figure 3. Division of the region into nodes and meshes.

Substituting values of a, b, and c into Equation (10) to get $H_e(x, y)$ as:

$$H_e(x,y) = [1 \quad x \quad y]\frac{1}{2A}\begin{bmatrix}(x_2y_3 - x_3y_2) & (x_3y_1 - x_1y_3) & (x_1y_2 - x_2y_1)\\ (y_2 - y_3) & (y_3 - y_1) & (y_1 - y_2)\\ (x_3 - x_2) & (x_1 - x_3) & (x_2 - x_1)\end{bmatrix}\begin{bmatrix}H_{e1}\\ H_{e2}\\ H_{e3}\end{bmatrix} \tag{13}$$

The magnetic field intensity derived for one finite element can be applied to the rest of the elements and thus can be solved as a weighted residual method. In this case, the weighted functions are the same as the shape functions for triangular shaped finite elements. Thus, if we assume any finite element, n inside the region with three nodes, i, j, k, then using Equation (10), the element shape function can be expressed as

$$N_n(x,y) = \frac{a_n + b_n x + c_n y}{2A} \tag{14}$$

where

$$\begin{array}{lll} a_i = x_j y_k - x_k y_j, & a_i = x_j y_k - x_k y_j, & c_i = x_k - x_j \\ a_j = x_k y_i - x_i y_k, & b_j = y_k - y_i, & c_j = x_i - x_k \\ a_i = x_i y_j - x_j y_i, & b_k = y_i - y_j, & c_k = x_j - x_i \end{array} \tag{15}$$

and A is the area of triangular element. A method of weighted residual is applied by integrating the partial differential equation over a region S

$$\int_S N_n \left(\left(\frac{\partial}{\partial x}\right)\left(\frac{1}{\mu}\frac{\partial H}{\partial x}\right) + \left(\frac{\partial}{\partial y}\right)\left(\frac{1}{\mu}\frac{\partial H}{\partial y}\right)\right) dS - \int_S N_n \left(j\omega\sigma - \omega^2\varepsilon\right) H dS = 0 \tag{16}$$

and can also be expressed in matrix form as

$$[M + K]H = 0 \tag{17}$$

$$M = (j\omega\sigma - \omega^2\varepsilon)\int_S N_n N_m dS$$

$$K = \frac{1}{\mu}\int_S \left(\frac{\partial N_n}{\partial x}\frac{\partial N_m}{\partial x} + \frac{\partial N_n}{\partial y}\frac{\partial N_m}{\partial y}\right) dS$$

$$= \frac{1}{4\mu A}\begin{bmatrix} b_ib_i + c_ic_i & b_ib_j + c_ic_j & b_ib_k + c_ic_k \\ b_ib_j + c_ic_j & b_jb_j + c_jc_j & b_jb_k + c_kc_k \\ b_ib_k + c_ic_k & b_jb_k + c_jc_k & b_kb_k + c_kc_k \end{bmatrix} \tag{18}$$

The above 3×3 matrix is an approximation for one element with 3 nodes. For the circular region of three-phase circuit divided into n nodes, the system equation will be an $n \times n$ matrix. The circular area under study is thus converted into a fine mesh with large number of nodes and finite elements.

3.2. Boundary Conditions and Simulation Parameters for FEM Model

The equations described in Section 3 are integrated over each finite element to calculate the magnetic field per finite element and thus for the whole selected region. The function parameters can vary at each edge and node, and therefore, there is a need to define the value at the vertex and edge of each element. This is solved by applying Dirichlet boundary condition by which a specified value of potential is assigned as a linear function of coordinates. The function parameters are adjusted to avoid the discontinuity at the edge. The finite element formulation is applied to the circular region with a radius of 200 cm for triangular structures as shown in Fig. 2. The region is divided into 20,000 finite elements, and the number of iterations is fixed to ten. This gives a total populated magnetic field for the circular region surrounding the structure.

4. MAGNETIC FIELD AT SPECIFIC DISTANCES FROM CONDUCTORS

The values of magnetic fields expressed by Equation (3) can be even more accurate if the measurement points around the current carrying conductor are increased. The resulting magnetic field will then be an addition of fields produced by three currents at multiple points situated together and will depend on the distance of these points from each conductor. This difference in these distances can be considered either in one dimension or two dimensions. One of such arrangements is shown in Fig. 1. The number of points can be anywhere near the current carrying conductor and at any angle. The field intensity captured at more points results into gaining more detailed information about the dynamically changing magnetic field at every change in the phase angle and time. Let us consider that the measurement points P1, P2, and P3, up to P36 are situated at certain distances with equal spacing between each other in four directions perpendicular to each other around each phase conductor as shown in Fig. 4 given below. The magnetic fields can be calculated at multiple points for each phase conductor. The equations of the magnetic flux density for all 36 points by using Equation (3) are expressed as follows:

$$
\begin{aligned}
B_{\mathrm{P1}}(I,t) &= \sum_{t=1}^{n}\sum_{\theta=1}^{\theta=360}\left\{\frac{\mu_0}{2\pi d_{11}}\left(I_{A_\theta},t\right)+\frac{\mu_0}{2\pi d_{12}}\left(I_{B_{\theta-120}},t\right)+\frac{\mu_0}{2\pi d_{13}}\left(I_{C_{\theta+120}},t\right)\right\}\\
B_{\mathrm{P2}}(I,t) &= \sum_{t=1}^{n}\sum_{\theta=1}^{\theta=360}\left\{\frac{\mu_0}{2\pi d_{21}}\left(I_{A_\theta},t\right)+\frac{\mu_0}{2\pi d_{22}}\left(I_{B_{\theta-120}},t\right)+\frac{\mu_0}{2\pi d_{23}}\left(I_{C_{\theta+120}},t\right)\right\}\\
B_{\mathrm{P3}}(I,t) &= \sum_{t\ =1}^{n}\sum_{\theta=1}^{\theta=360}\left\{\frac{\mu_0}{2\pi d_{31}}\left(I_{A_\theta},t\right)+\frac{\mu_0}{2\pi d_{32}}\left(I_{B_{\theta-120}},t\right)+\frac{\mu_0}{2\pi d_{33}}\left(I_{C_{\theta+120}},t\right)\right\}\\
B_{\mathrm{P4}}(I,t) &= \sum_{t=1}^{n}\sum_{\theta=1}^{\theta=360}\left\{\frac{\mu_0}{2\pi d_{41}}\left(I_{A_\theta},t\right)+\frac{\mu_0}{2\pi d_{42}}\left(I_{B_{\theta-120}},t\right)+\frac{\mu_0}{2\pi d_{43}}\left(I_{C_{\theta+120}},t\right)\right\}\\
&\vdots\\
&\vdots\\
B_{\mathrm{P36}}(I,t) &= \sum_{t=1}^{n}\sum_{\theta=1}^{\theta=360}\left\{\frac{\mu_0}{2\pi d_{361}}\left(I_{A_\theta},t\right)+\frac{\mu_0}{2\pi d_{362}}\left(I_{B_{\theta-120}},t\right)+\frac{\mu_0}{2\pi d_{363}}\left(I_{C_{\theta+120}},t\right)\right\} \qquad (19)
\end{aligned}
$$

These points of measuring the magnetic field from center of each conductor have a purpose of capturing magnetic field which decreases with increasing distance. This information is then used to calculate current in each phase. As described in Fig. 4, a set of twelve measurement points for each phase is assigned. For convenience of the definition of variables in MATLAB program, we assign numbers to these points with a group of three in East(E), West(W), North(N), and South(S) directions. This convention will be used for the programming and analysis in both medium and high voltage cases. For a selected point from P1 to P36, there are three distances of that particular point from each phase. These distances are calculated from the right angle geometry for each point from three phases and are also mentioned in Equation (19). For example, for point P1, the distances from phase A, B, and C are d_{11}, d_{12}, and d_{13} respectively. Similarly, for point P2, the distances are d_{21}, d_{22}, and d_{23}.

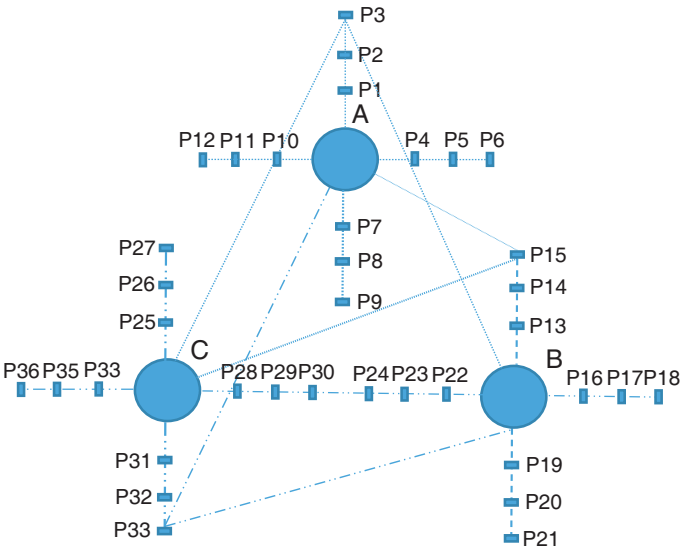

Figure 4. Measurement points for each phase.

5. LINEAR REGRESSION ANALYSIS TO ESTIMATE THREE-PHASE CURRENTS

For all points of measurement, the magnetic field equation shows a linear relation between the known and unknown variables. Therefore, the estimation of instantaneous values of current from measured field values can be achieved by applying linear regression technique. In this method, the magnetic field and distances are assigned to be the known co-variables and currents as response variables. The linear regression function f from n covariables and their responses are expressed as

$$B = f(X_i) + \xi \tag{20}$$

here, ξ is the noise in the measurements. For a certain number of parameters, $\beta = (\beta_1, \ldots, \beta_p)^T$, the estimates of β that minimizes the residual sum of squares is expressed as:

$$f(\beta_1, \ldots, \beta_p) = \sum_{i=1}^{n} \left(B_i - \sum_{j=1}^{p} x_{ij}\beta_j \right)^2 \tag{21}$$

where $x_{ij} = (x_{i1}, x_{i2}, \ldots, x_{ip})^T$ for $j = 1, \ldots, p$ is a vector of feature measurements for the ith sensor.

In order to define the estimator for the linear regression model of currents, it is worth to write the equations from Eqs. (8), (10), and (11) into matrix notation. Then the magnetic field response values will be converted into a matrix, B, and feature values will be converted into a matrix, X, as follows

$$B = \begin{bmatrix} B_{p1} \\ B_{p2} \\ \vdots \\ B_{pn} \end{bmatrix}, \quad \text{and} \quad X = \begin{bmatrix} x_{11} & x_{12} & \cdots & x_{1p} \\ x_{21} & x_{22} & \cdots & x_{2p} \\ \vdots & \vdots & \ddots & \vdots \\ x_{n1} & \mathrm{x}_{n2} & \cdots & x_{np} \end{bmatrix} \tag{22}$$

Equation (10) is then written as

$$f(\beta) = (B - X\beta)^T (B - X\beta) \tag{23}$$

The derivative of above equation also given in Equation (11) when being divided by -2 becomes

$$B^T X = \hat{\beta}^T X^T X \tag{24}$$

Taking transpose on both sides of above equation and rearranging, we get

$$\left(X^T X\right)^T \hat{\beta} = X^T B \tag{25}$$

It is observed that all columns in the X matrix are linearly independent, and therefore this matrix has full rank. Moreover, the XTX matrix is non-singular, and therefore, above equation can be written as follows:

$$\hat{\beta} = \left(X^T X\right)^{-1} X^T B \tag{26}$$

The above Equation (26) gives the estimates of three-phase currents. The least squares estimation technique gives the estimated values after minimizing the error function based on covariables matrix and the observed response values of magnetic fields. The computation program for regression analysis using these equations of magnetic fields is developed in MATLAB and is applied to various combinations of distances with specific application to triangular structures in medium voltage and high voltage cases.

6. ESTIMATION OF CURRENTS FOR MEDIUM VOLTAGE THREE-PHASE SYSTEM

The source for generating current is defined as a time-varying low frequency three-phase balanced source with variation of phase angle from 0° to 360° with time steps of 0.00001 seconds. The equations for each phase source are $V_A = 12470\sqrt{\frac{2}{3}}\sin(360 * 60 * t)$, $V_B = 12470\sqrt{\frac{2}{3}}\sin(360 * 60 * t - 120)$, and $V_C = 12470\sqrt{\frac{2}{3}}\sin(360 * 60 * t + 120)$. The impedance of the ACSR conductors is set to 3.386 Ω. Magnetic fields are calculated at points of interest from Fig. 4. As explained in Section 4, each point will have three distances from phase A, B, and C. For example, for point P1, the distances d_{11}, d_{12}, and d_{13} are calculated from the triangular geometry with reference to point P1's location at 2.5 cm in the North. Similarly, the distances for points in other three directions are calculated accordingly. Selected points are at the distances of 2.5 cm, 5 cm, and 7.5 cm form each phase. These distances are inserted in Equation (19) to calculate the magnetic field for each individual point for selected combinations. The measured values of magnetic fields are then used in the second part of the algorithm to calculate the currents using the Least Squares method. The simulation parameters explained in Section 4 generate three phase balanced currents of magnitude 150 A per phase as shown in Fig. 5. The study of magnetic field and current estimation is organized into three groups. Group I has all combinations of the measurement points for three conductors with only one point per phase. Group II has two measurement points, and Group III has three points per phase by using all 36 points shown in Fig. 4. Various combinations include selecting each point from one direction for each phase. Among various combinations tried for each group, only the best and worst results are shown in Table 1. Magnetic field generated from the source currents for each phase is shown in Fig. 6. The instantaneous values of currents are in amperes, and magnetic fields for each phase have the unit of Tesla.

As seen from Table 1, the first column gives all combinations which give the maximum and minimum errors in current estimation. The second to fourth columns give the measurement points from each

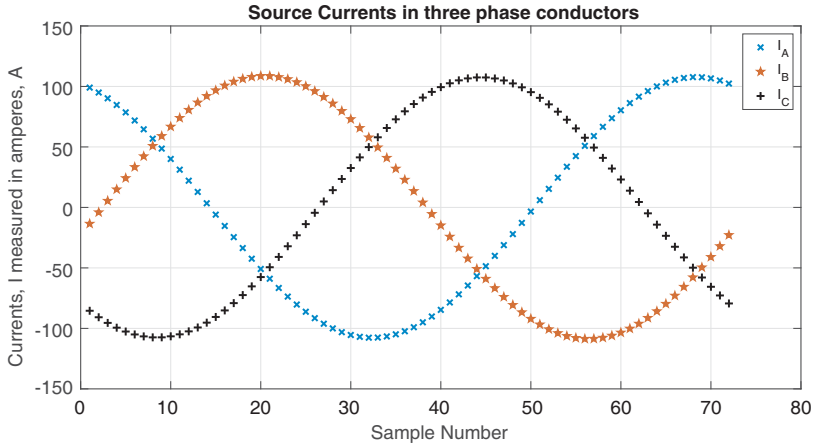

Figure 5. Three phase currents in Amperes for 12.47 kV.

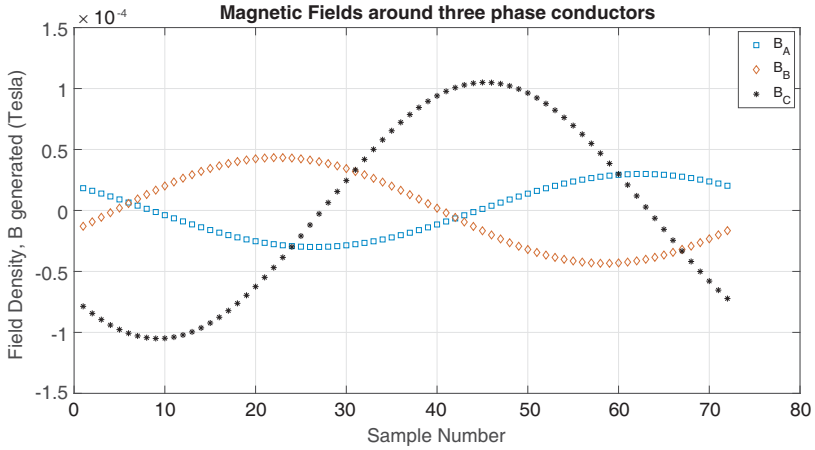

Figure 6. Three phase magnetic field density for 12.47 kV.

Table 1. Estimated current errors in percentage for medium voltage triangular arrangement of conductors.

Groups and Combinations	Measuring Pts From Ph A	Measuring Pts From Ph B	Measuring Pts From Ph C	% Est error $I_{A_{error},Max}$	% Est error $I_{B_{error},Max}$	% Est error $I_{C_{error},Max}$
Group I: One Point						
I.1	P1	P16	P34	3.18	3.48	1.67
I.2	P2	P17	P35	1.62	1.74	3.51
I.3	P1	P19	P31	3.07	2.73	3.37
I.4	P1	P19	P34	2.98	2.67	1.93
I.5	P4	P19	P34	2.55	2.69	1.90
I.6	P9	P21	P33	11.40	8.90	7.80
I.7	P12	P24	P36	12.11	11.8	4.47
I.8	P6	P18	P30	15.84	7.76	12.63
Group II: Two Points						
II.1	P1, P2	P16, P17	P34, P35	2.76	3.35	7.72
II.2	P1, P2	P19, P20	P34, P35	2.54	3.09	4.59
II.3	P1, P3	P19, P21	P34, P36	2.55	3.01	4.56
II.4	P2, P3	P19, P20	P31, P32	2.06	2.71	3.72
II.5	P8, P9	P20, P21	P32, P33	10.44	5.13	6.28
II.6	P11, P12	P23, P24	P35, P36	9.92	8.71	3.23
Group III: Three Points						
III.1	P1, P2, P3	P16, P17, P18	P34, P35, P36	2.83	3.43	5.31
III.2	P1, P2, P3	P19, P20, P21	P31, P32, P33	2.68	3.26	4.18
III.3	P7, P8, P9	P19, P20, P21	P31, P32, P33	6.34	2.79	4.13
III.4	P10, P11, P12	P22, P23, P24	P34, P35, P36	7.25	4.24	3.01

phase. Last three columns give errors in amperes. It is observed from this table that the errors are minimum for points closer to conductors and increase for points farther from the conductors. Therefore, the best results are obtained when the distance combinations use 2.5 cm for single, double, and three

measurement points. This is evident from cases I.3 and I.4 for single point measurements, II.3 and III.1 cases for two and three points combinations. The minimum error in amperes is 0.89 A, and the best combination is I.3 for Group I. Similarly, for Group II, the minimum error combination has 1.24 A, 1.53 A, and 1.07 A for phases A, B, and C, respectively. For three point measurement group, the estimation error is $I_A = 1.38$ A, $I_B = 2.77$ A, and $I_C = 1.25$ A. All of these cases, when being referred to Fig. 4, indicate that these points are placed very close to each phase. The minimum error of estimation is found to be 1.67%, and the maximum error is found to be 15.84%. The maximum error is for the point at 7.5 cm from phase A conductor. It is also clear from this table that the error goes on decreasing with the increased number of measurement points per phase.

Moreover, the results of case II.2 show that when two points per phase are used in the direction, such as North, South, and West, then the magnetic field sensing and current calculation is improved. The maximum error is found in case II.5 with the magnitudes of 11.14 A, 4.14 A, and 5.35 A for each phase. This is because the combination has points at 7.5 cm. The error for phase A is 11.14 A, because the field generated by phase A has interference with those generated by phases B and C. As a result, the magnetic field value itself is less and not the true representation of the actual current flowing in phase A conductor. The estimation errors for the rest of two phases are less, because the points are in South direction of the phases and sufficiently away from each other not to have any interference of neighboring magnetic fields. There is a pattern of reduced error for the same combination in Group III where the measurement points per phase are three and thus increase the accuracy of the estimation algorithm.

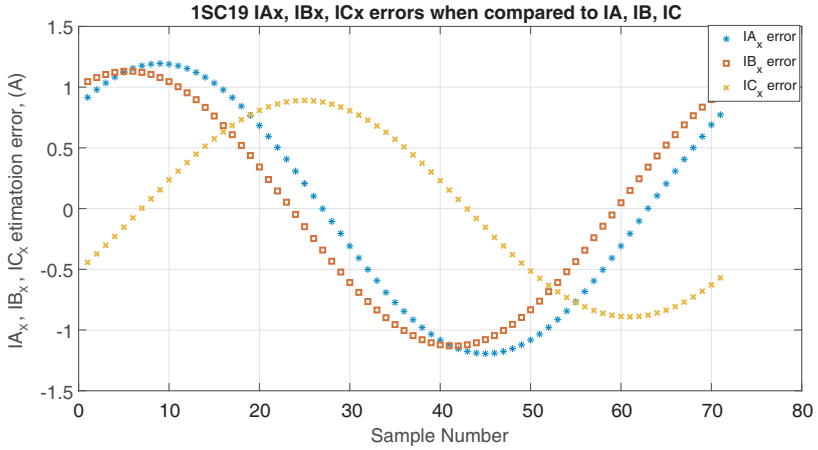

Figure 7. Errors in $I_A(t)$, $I_B(t)$ and $I_C(t)$ in Amperes for case I.4.

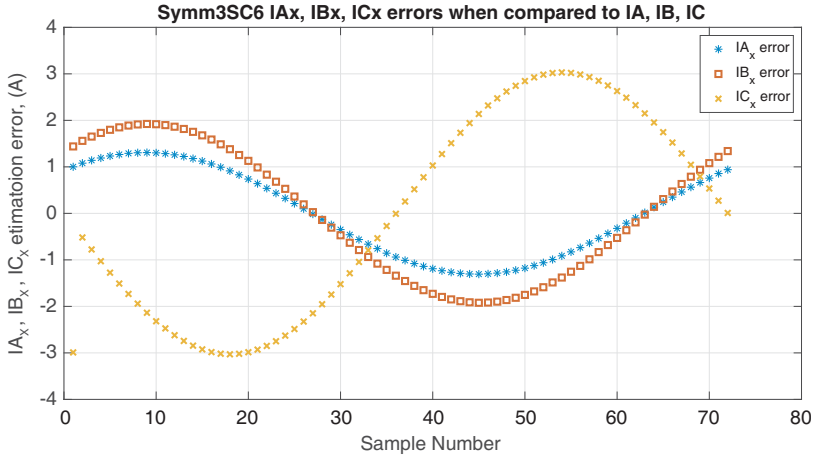

Figure 8. Errors in $I_A(t)$, $I_B(t)$, and $I_C(t)$ in Amperes for Case III.2.

The estimation errors as result of the algorithm for each phase for case I.4 and III.2 are shown in Fig. 7 and Fig. 8. The computational accuracy for the approximation of the magnetic field is higher for Group III, where there are three points of measurement per phase. There were in total six combinations tried for three points per phase case. The errors are minimum considering the greater number of samples for each iteration of the algorithm.

7. ESTIMATION OF CURRENTS FOR HIGH VOLTAGE THREE-PHASE SYSTEM

In this case, the algorithm and computational code remain the same as that for medium voltage. The simulation parameters are changed for the source potentials to give higher magnitudes of three-phase balanced voltages with phase difference of 120°. Other parameters such as number of nodes, number of finite elements, sampling time, and range of phase angle variation are kept at same values as previous case. The structure is considered as triangular with phase A at the top of the triangle and phase B and phase C on the base of the triangle. The conductor specifications are ACSR 556 mcm single conductor per phase. Similarly, there are three groups, single point, two points, and three points at the same distances of 2.5 cm, 5 cm, and 7.5 cm from the center of each conductor. Similar combinations are selected as those of the previous cases. Moreover, the values considered for the distances between each phase and the points of measurement are similar to those considered for the previous case. The results for the best cases are shown in Table 2.

In this case of simulation for high voltage, the alternating currents generated have the magnitude of 1200 A with a low frequency of 60 Hz. Therefore, the magnetic fields generated also have higher magnitude, and accordingly the algorithm estimates the currents from these magnetic fields. The errors

Table 2. Estimated current errors in percentage for medium voltage triangular arrangement of conductors.

Groups and Combinations	Measuring Pts From Ph A	Measuring Pts From Ph B	Measuring Pts From Ph C	% Est error $I_{A_{error},Max}$	% Est error $I_{B_{error},Max}$	% Est error $I_{C_{error},Max}$
Group I: One Point						
I.1	P1	P13	P25	2.98	3.55	3.00
I.2	P3	P15	P27	2.62	4.45	3.84
I.3	P1	P16	P34	3.10	1.98	3.39
I.4	P2	P17	P35	1.10	12.6	31.88
I.5	P12	P24	P36	10.39	12.82	3.92
I.6	P6	P18	P30	10.55	4.52	12.78
Group II: Two Points						
II.1	P1, P3	P13, P15	P25, P27	2.62	4.45	3.84
II.2	P1, P2	P16, P17	P34, P35	2.49	2.13	2.98
II.3	P2, P3	P17, P18	P35, P36	0.286	6.55	8.43
II.4	P2, P3	P14, P15	P26, P27	0.74	8.74	8.89
II.5	P5, P6	P17, P18	P29, P30	8.03	3.94	9.45
II.6	P8, P9	P20, P21	P32, P33	9.50	6.98	6.28
Group III: Three Points						
III.1	P1, P2, P3	P13, P14, P15	P25, P26, P27	2.095	5.09	4.43
III.2	P1, P2, P3	P16, P17, P18	P34, P35, P36	2.25	2.24	2.72
III.3	P10, P11, P12	P22, P23, P24	P34, P35, P36	4.54	5.27	2.60
III.4	P7, P8, P9	P19, P20, P21	P31, P32, P33	5.22	1.52	3.59

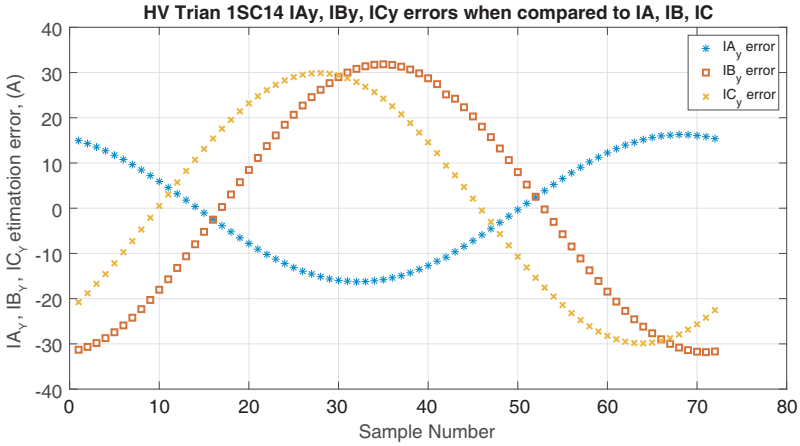

Figure 9. Errors in $I_A(t)$, $I_B(t)$ and $I_C(t)$ in Amperes for HV case I.2.

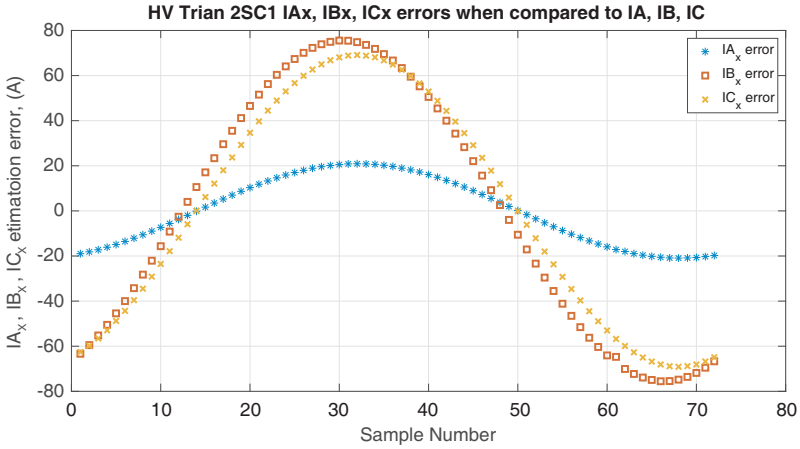

Figure 10. Errors in $I_A(t)$, $I_B(t)$ and $I_C(t)$ in Amperes for HV case II.3.

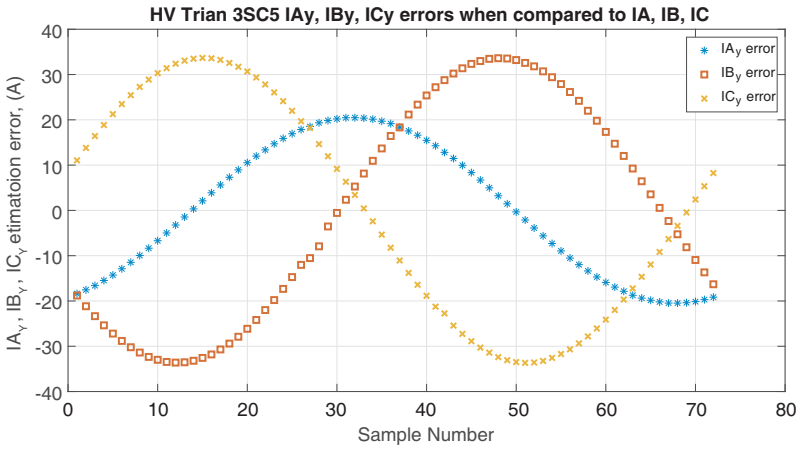

Figure 11. Errors in $I_A(t)$, $I_B(t)$ and $I_C(t)$ in Amperes for HV case III.1.

between calculated and original currents for three cases are plotted as shown in Fig. 9, Fig. 10, and Fig. 11. In this category too, it is observed that higher number of points of measurement per phase decreases the error in estimation. This is backed by the results shown in Table 2. For the limitation of

pages of the article, results for all combinations are not shown. Only the best and worst case results are shown. The estimation error is maximum in cases where the points are away from the conductors, and it is minimum when the points are closer to the conductors. There are cases such as I.5 where all three points are at 7.5 cm and give estimated currents as $I_A = 160.61$ A, $I_B = 238.45$ A, and $I_C = 60.60$ A resulting into maximum values of percentage error of 10.39%, 12.82%, and 3.92%. These results are similar to that of case I.6 where three points of measurements are 7.5 cm to the East of each conductor. This proves that the accuracy of estimation decreases with increasing distance from the conductors. The maximum percentage error in estimation of currents is calculated to be 15.84%, and the minimum error value is 1.67%. Table 2 shows that the results of cases II.3 and III.2 are similar with a slight improvement in the accuracy for III.2. This means that addition of the third measurement point at 7.5 cm did not contribute much to the results of two points at 2.5 cm and 5 cm in the same direction for each phase.

8. CONCLUSION AND DISCUSSION

The simulation and modeling of the magnetic field to estimate the currents in each individual phase are successfully performed using least squares algorithm in MATLAB. This research is based on the Maxwell's second order differential equations which are also proven to be useful in previous studies. The contribution of this research is an additional step towards the use of magnetic field. The results obtained for various combinations in triangular arrangements have shown that there is a strong relation between the magnetic field near the conductors and the currents and knowing the first, the second can be calculated with least errors of estimation. The best and worst case results for all three groups and cases for both medium voltage and high voltage are recorded and given in the tables. The maximum or peak values of percentage errors from the samples out of one cycle for the worst cases are found to be 15.84% and the rms value to be 11.02% rms. Conventional current transformers (CTs) used for protection relaying purpose have an accuracy of $\pm 10\%$ rms [2]. These CTs are grouped in T class and C class, and their accuracy depends on the primary to secondary transformation ratio. Comparing our method with the performance of these CTs, the percentage error for most of the cases is below 4.14% rms which is comparatively better than that of the conventional C and T class CTs. The worst case interaction between the magnetic fields of neighboring conductors acts negating the magnitude generated by each individual. This fact was already considered, and therefore, this study emphasizes to measure or sense the field at various distances with various combinations of the points in four directions perpendicular to each conductor. The best case results show that there is a specific combination of the locations from each phase which helps in minimum overlapping of the neighboring magnetic fields, and the currents can be calculated with maximum accuracy. The least squares method with residual error function is proven to be successfully applicable to calculate individual currents from mixed magnetic fields. The worst case results show that fields weaken with increased distance and also because of interference of neighboring fields. Moreover, it is observed that the measurement accuracy increases with the number of measurement points provided that they are closer to the conductors. This means that a set of measurement points as closer to each conductor gives better accuracy than those involving more distant points. The results for the combination of points at 2.5 cm and 5 cm give better results than the combination of points at 5 cm and 7.5 cm. This is because the farther the point form one conductor, the weaker is the magnetic field. The arrangement of three-phase conductors is another governing factor to calculation accuracy. In medium voltage case, it is observed that increasing measurement points reduces the estimation error, but this error shows increasing trend in the case of high voltage case. Increased number of measurement points in the same direction for each phase give higher error of estimation. However, the percentage of measurement does not vary much in all three cases. There is a difference of 5.2% in the accuracy between medium and high voltage current estimations. The combinations of the measurement points in this research are defined from the centre of the conductor for each type of ACSR conductor. Overall, it is observed that increasing the number of measurement points increases the estimation accuracy.

This research concludes to two major outcomes for future applications regarding sensing the magnetic field for estimation of currents, the first being that there is a specific combination of the directions for each sensing or measuring point for maximum accuracy. It is North, East, and West for

the triangular structure. The North direction is for phase A, East direction for phase B, and the West direction for Phase C conductor. Sensing points are away from the neighboring phases, and therefore there is minimum interference of the magnetic fields produced by neighboring phase conductors. The second outcome is that if there are two sensing points, one at 2.5 cm and the other at 5 cm, then they increase the current estimation accuracy. Therefore, the results of this research recommend use of a set of two magnetic field sensing points in North, East, and West directions each at 2.5 cm and 5 cm from each phase to achieve maximum accuracy in current estimation.

REFERENCES

1. Campbell, R. J., "Weather-related power outages and electric system resiliency," *CRS Report for Congress, Congressional Research Service*, 3–14, 7-5700, www.crs.gov, R42696, 2012.
2. IEEE Standard C37.110-2007, *IEEE Guide for the Application of Current Transformers Used for Protective Relaying Purposes*, IEEE Press, 2007.
3. Sadiku, M. N., *Numerical Techniques in Electromagnetics with MATLAB*, 3rd edition, CRC Press, 2012.
4. Tupsie, S., "Analysis of electromagnetic field using FEM for transmission lines transposition," *Journal Title Abbreviation*, Vol. 34, No. 10, 1064–1076, 2013.
5. Pao-La-Or, P., P. Isaramongkolrak, and P. Pao-La-Or, "Title of the journal paper," *International Journal of Electrical and Computer Engineering*, Vol. 3, No. 5, 1174–1178, 2009.
6. Hamayer, K., R. Mertens, and R. Belmans, "Computation and measurement of electromagnetic fields of AC-high voltage transmission lines," *Sixth International Conference on AC and DC Power Transmission*, 52–57, 1996.
7. Farah, A. A. M., M. M. Afonso, J. A. Vasconcelos, and M. A. O. Schroeder, "A finite-element approach for electric field computation at the surface of overhead transmission line conductors," *IEEE Transactions on Magnetics*, Vol. 54, No. 3, 1–4, 2018.
8. Pao-La-Or, P., T. Kulworawanichpong, and S. Sujitjorn, "Distributions of flux and electromagnetic force in induction motors: A finite element approach," *WSEAS Transactions on Systems*, Vol. 5, No. 3, 617–624, 2006.
9. Mismar, M., "Numercial simulation of Maxwell's equations," *IOSR Journal of Engineering*, Vol. 7, No. 3, 1–10, 2017.
10. Ray, W. F. and C. R. Hewson, "High performance Rogowski current transducers," *Proceedings of IEEE Industrial Applications Conference*, 3083–3090, Rome, Italy, 2000.
11. Ripka, P., "Electric current sensors: A review," *Measurement Science Technology*, Vol. 21, No. 112001, 1–23, 2010.
12. Ziegler, S., R. C. Woodward, H. H. C. Lu, and L. J. Borle, "Investigation into static and dynamic performances of the copper trace current sense method," *IEEE Sensors J.*, Vol. 9, No. 7, 782–791, 2009.
13. Honeywell, *Hall Effect Sensing and Application*, Honeywell, 2010.
14. Ripka, P., "Advances in fluxgate sensors," *Sensors and Actuators A*, Vol. 106, 8–14, 2003.
15. Lenz, J. and A. S. Edelstein, "Magnetic sensors and their applications," *IEEE Sensors J.*, Vol. 6, No. 3, 631–649, 2006.
16. D'Antona, G., L. Di Rienz, R. Ottoboni, and M. Manara, "Processing magnetic sensor array data for AC current measurement in multiconductor systems," *IEEE Transactions on Instrumentation and Measurement*, Vol. 50, No. 5, 1289–1295, 2001.
17. Dogaru, T. and S. T. Smithz, "Giant magnetoresistance-based eddy-current sensor," *IEEE Transactions on Magnetics*, Vol. 37, No. 5, 3831–3838, 2001.
18. USF Section 2 April 2017, *Voltages, Line Locations and Clearances for Distribution Circuits*, Utility Standards Forum.
19. USF Section 01–17 January 2017, *Overhead Primary Framing*, Utility Standards Forum.